

## The Sublimative Evolution of (486958) Arrokoth

Jordan K. Steckloff<sup>1,2</sup>

Carey M. Lisse<sup>3</sup>

Taylor K. Safrit<sup>4</sup>

Amanda S. Bosh<sup>4</sup>

Wladimir Lyra<sup>5</sup>

Gal Sarid<sup>6</sup>

<sup>1</sup>Planetary Science Institute, Tucson AZ

<sup>2</sup>University of Texas at Austin, Austin, TX

<sup>3</sup>Johns Hopkins University, Applied Physics Laboratory, Laurel, MD

<sup>4</sup>Massachusetts Institute of Technology, Cambridge, MA

<sup>5</sup>New Mexico State University, Las Cruces, NM

<sup>6</sup>SETI Institute, Mountain View, CA

### Abstract

We consider the history of *New Horizons* target (486958) Arrokoth in the context of its sublimative evolution. Shortly after the Sun's protoplanetary disk (PPD) cleared, the newly intense sunlight sparked a sublimative period in Arrokoth's early history that lasted for  $\sim 10 - 100$  Myr. Although this sublimation was too weak to significantly alter Arrokoth's spin state, it could drive mass transport around the surface significant enough to erase topographic features on length scales of  $\sim 10 - 100$  m. This includes craters up to  $\sim 50 - 500$  m in diameter, which suggests that the majority of Arrokoth's craters may not be primordial (dating from the merger of Arrokoth's lobes), but rather could date from after the end of this sublimative period. Thereafter, Arrokoth entered a Quiescent Period (which lasts to the present day), in which volatile production rates are at least 13 orders of magnitude less than the  $\sim 10^{24}$  molecules/s detection limit of the *New Horizons* spacecraft (*Lisse et al. 2020*). This is insufficient to drive either mass transport or sublimative torques. These results suggest that the observed surface of Arrokoth is not primordial, but rather dates from the Quiescent Period. By contrast, the inability of sublimative torques to meaningfully alter Arrokoth's rotation state suggests that its shape is indeed primordial, and its observed rotation is representative of its spin state after formation.

## I. Introduction

(486958) Arrokoth is a cold classical Kuiper Belt Object (KBO), which is thought to have formed at 44.6 au from the Sun, where it has resided ever since (*Stern et al. 2019*). This stability is unique amongst all objects previously visited by spacecraft, which are thought to have moved and migrated due to instabilities among the giant planets and disk-planet interaction after formation. Thus, Arrokoth provides an opportunity to study how thermally driven processes could have evolved this object over the age of the Solar System, from formation in the Sun's protoplanetary disk (PPD) to the present. Because Arrokoth is rich in ices (*Grundy et al. 2020; Lisse et al. 2020*), early sublimative processes could have dramatically altered its surface features and appearance, and even its behavior if vigorous enough, e.g. affecting the spin state of the body via the effects of sublimative torques. Indeed, such processes could be quite important in the evolution of Arrokoth, which (i) is thought to have formed from a gentle merger of two separate objects that bled off significant orbital and rotational angular momentum (*Hirabayashi et al. 2020, McKinnon et al. 2020*) and (ii) shows sufficient crater counts to date its surfaces to the earliest part of the Solar System's history (*Spencer et al. 2020*). Here we explore how sublimative activity may have affected Arrokoth over its history.

## II. Periods of Arrokoth's History

Arrokoth formed in extremely cold conditions in the Sun's protoplanetary disk (PPD), sufficient for CO (*Krijt et al. 2018*) and other hypervolatile species (such as N<sub>2</sub>, and CH<sub>4</sub>) to condense into solids. Later, the Sun's T Tauri winds and gas accretion cleared out the protoplanetary disk (PPD); Arrokoth's surface was newly exposed to solar heating. At this point, the surface of Arrokoth was likely pristine, with hypervolatile CO, N<sub>2</sub>, and CH<sub>4</sub> present (*Lisse et al. 2020*). The sublimation rate of these ices would have been very high, representing a maximum sublimative flux from the surface. However, as these volatiles sublimated away and depleted the body, Arrokoth would eventually cease to vigorously outgas, and would enter a steady state sublimative regime that exists to the present day. For this reason, we must separately consider these two periods: the "Sublimative Period" (shortly after the clearing of the Sun's PPD), and the "Quiescent Period" (began once Arrokoth reached a thermodynamic steady state).

*Arrokoth's Sublimative Period*

We can estimate the duration of the Sublimative Period by computing how long the post PPD thermal wave would require to reach the center of the body (and hence the time after which the primitive thermal structure is lost). Although there has been some advancement in past work regarding the thermophysical evolution of KBO surfaces and interiors, there are still many basic open questions, large parameter uncertainties, and a lack of constraints for ranges of physical parameters. Specific to our modeling work in this paper are the important issues of object size, density, and assumed composition. In many respects, while Arrokoth is clearly a member of the cold-classical KBO dynamical grouping, its size and probable density of  $\sim 300 - 500 \text{ kg/m}^3$  (Hirabayashi *et al.* 2020; McKinnon *et al.* 2020) is physically most akin to a large comet nucleus (e.g., Richardson *et al.* 2007; Thomas *et al.* 2013; Patzold *et al.* 2016, Kokotanekova *et al.* 2017; Pruesker *et al.* 2017). The two distinct lobes may even be considered as proxies for two small comet nuclei (roughly 7.5 and 10 km in radius), as their internal thermal evolution has probably initiated and progressed with minimal cross-influence in the deep interior, similarly to other small icy bodies (e.g., Davidsson *et al.* 2016, McKinnon *et al.* 2020).

In contrast, previous work dealing with the thermophysical evolution of KBOs has largely focused on significantly larger objects with higher densities than Arrokoth (e.g., De Sanctis *et al.*, 2001, 2007; Merk & Prialnik, 2003; Choi *et al.*, 2002; Prialnik *et al.* 2008; Sarid & Prialnik, 2009; Desch *et al.* 2009; Guilbert-Lepoutre *et al.* 2011). Although some of the studied examples are only an order of magnitude greater in volume than Arrokoth (e.g., De Sanctis *et al.* 2001; Prialnik *et al.* 2008; Sarid & Prialnik, 2009), these examples are nevertheless much too large to be applicable to Arrokoth; especially in the effects of radiogenic heating, for which the amplitude of heating depends directly on size. The net thermal energy deposition results from a balance between heat loss through the surface and heat production within the interior. Thus, the smaller the object's radius, the lower the maximum temperature it can attain. Indeed, while sophisticated models exhibit the dependence on size, density, composition, and radionuclide abundance, many studies of icy body radiogenic heating have shown that the amplitude of this effect is negligible for water ice rich bodies (mostly in mixed crystalline and amorphous form) with radii smaller than  $\sim 10\text{-}15 \text{ km}$  (e.g., Prialnik & Podolak 1995; De Sanctis *et al.* 2001; Choi *et al.* 2002; Prialnik *et al.* 2008, Sarid & Prialnik 2009).

To estimate the characteristic timescale of the Sublimative Period, we rearrange the thermal skin depth equation, which measures the distance below the surface at which the amplitude of a surface thermal wave decreases by  $1/e$ :

$$d_{skin} = \sqrt{\mathcal{H}t} \quad (1)$$

$$t = \frac{d_{skin}^2}{\mathcal{H}} \quad (2)$$

where  $d_{skin}$  is the thermal skin depth,  $\mathcal{H}$  is the thermal diffusivity, and  $t$  is the elapsed time. Thermal diffusivity measures the ease with which a heat wave diffuses into a surface, and is related to the thermal conductivity ( $k$ ), specific heat capacity ( $c_p$ ), and density ( $\rho$ ) by

$$\mathcal{H} = \frac{k}{\rho c_p}. \quad (3)$$

For Arrokoth, we use its most plausible density range of  $\sim 300 - 500 \text{ kg/m}^3$  (Hirabayashi *et al.* 2020; McKinnon *et al.* 2020), and the specific heat capacities for volatile ices, which are on the order of  $\sim 2000 \text{ J/kg K}$  (the specific heat capacity of water ice). The thermal conductivity of porous cometary material is on the order of  $\sim 10^{-2} - 10^{-1} \text{ W/K m}$  (Gundlach & Blum, 2012), resulting in a thermal diffusivity of  $\sim 10^{-8} - 10^{-7} \text{ m}^2/\text{s}$ .

Alternatively, thermal inertia ( $I$ ), which measures a surface's resistance to changing its temperature in response to a changing thermal environment, is related to thermal conductivity, specific heat capacity, and density by

$$I = \sqrt{k\rho c_p} \quad (4)$$

thus

$$\mathcal{H} = \frac{I^2}{\rho^2 c_p^2}. \quad (5)$$

The thermal diffusivity of the surface of Comet 67P/Churyumov-Gerasimenko is  $80_{-40}^{+80} \text{ JK}^{-1}\text{m}^2\text{s}^{-0.5}$  (Marshall *et al.* 2018) with a density of  $537.8 \pm 0.7 \text{ kg/m}^3$  (Pruesker *et al.* 2017), with a specific heat capacity modeled to be around  $\sim 350$  (Grundy *et al.* 2020) to  $\sim 1000 \text{ J kg}^{-1}\text{K}^{-1}$  (Hu *et al.* 2017),  $2 \times 10^{-8}$  ( $6 \times 10^{-9} - 9 \times 10^{-8}$ )  $\text{m}^2/\text{s}$ , which is consistent with this range of thermal diffusivities.

These values are smaller than the thermal diffusivities of typical geological materials ( $\sim 10^{-6} \frac{\text{m}^2}{\text{s}}$ ; Drury, 1987) due to the low densities and high porosities of small icy bodies<sup>1</sup>. From this

---

<sup>1</sup> Grundy *et al.* (2020) assumed thermal properties that recreate ground-based observations of KBOs, but result in thermal diffusivity values 3-4 orders of magnitude small still, which would result in the Sublimative Period lasting for  $\sim 100 \text{ Gyr}$

thermal diffusivity range, the thermal wave of the Sun would reach the centers of Arrokoth’s lobes  $\sim 10 - 100$  Myr after the dispersal of the PPD. This calculation assumes that the clearing of the PPD occurred instantaneously. While this is not strictly true (and indeed was likely to have occurred over a timescale of up to a few million years; *Williams & Cieza, 2011*), this is sufficiently short to not affect these order of magnitude estimates of Arrokoth’s Sublimative Period duration.

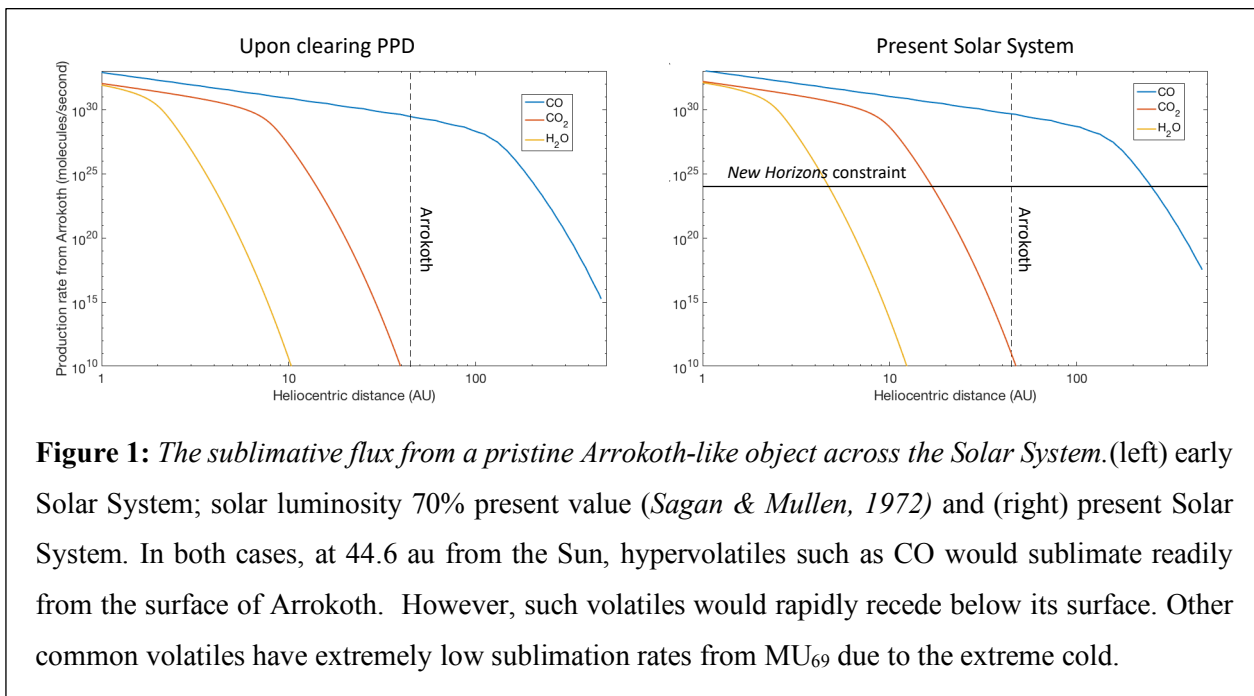
It is important to remember that the two lobes of Arrokoth have a smaller effective radius than their long-axis radius. When considering a more realistic representation of the “flat ellipsoid” shape of Arrokoth’s lobes (*McKinnon et al. 2020*), we can expect the internal thermal evolution to be less secular and advance in a more episodic pattern and at a faster rate at different locations within the body, especially if internal inhomogeneities are present (*e.g. Rosenberg & Privalnik 2010, Guilbert-Lepoutre et al. 2016*). Hence, these thermal evolution timescales are likely an estimate for the upper limit of the volatile-active, sublimative period, in Arrokoth’s evolution.

During the Sublimative Period, some volatiles outgassed vigorously, while others maintained extremely low production rates. To compute the sublimative flux of these volatiles, we use the model of *Steckloff et al. (2015)*, which solves the energy balance equation at the surface of the body, accounting for solar heating, and both radiative and sublimative cooling. This model uses first principles (Clausius-Clapyron relation, Langmuir-Knudsen equation of sublimation rates [*Langmuir, 1913*], conservation of energy, and conservation of momentum) to solve for the sublimative molecular flux and sublimative back reaction pressure exerted on the surface. Using this model, we can constrain the sublimative flux of CO from the surface of Arrokoth to up to  $\sim 4 \times 10^{29}$  molecules per second.  $N_2$  ice would behave similarly to CO (*Lisse et al. 2020*). Due to their much higher enthalpy of sublimation, sublimative cooling from other common icy volatiles such as  $H_2O$  and  $CO_2$  are at least eighteen orders of magnitude lower at 44.6 AU, Arrokoth’s distance from the Sun (see figure 1), and are therefore insignificant in the Sublimative Period. Thus, Arrokoth would effectively cease to outgas vigorously once depleted of CO and other minor supervolatiles.

### *Arrokoth’s Quiescent Period*

Once the thermal wave and supervolatile sublimation fronts reach Arrokoth’s center, the supervolatiles will be depleted, ending Arrokoth’s Sublimative Period. More refractory volatiles (*e.g.,  $CO_2$ ,  $H_2O$* ) would still be present within Arrokoth, however temperatures would be much too

low to allow these volatiles to sublimate vigorously. Instead, volatiles will slowly be released from the volatile sublimation fronts, diffuse to the surface, and ultimately leave the body. The rate of volatile loss (and thus rate of sublimation front recession) would depend on the relative volatility of the species. For Example, CO<sub>2</sub>'s high volatility would cause this species to recede faster into the surface than H<sub>2</sub>O. Eventually, these differences would be expected to produce a mature equilibrium subsurface structure on Arrokoth, similar to the expected subsurface structures of comets (*Prialnik et al. 2004*). Although these volatile fronts would continue to recede into Arrokoth, their extremely low outgassing rates (figure 1) suggests that this structure has changed little since formation (volatile fronts moved on the order of centimeters over the age of the solar system). Ultimately, the state observed by the *New Horizons* spacecraft is likely representative of the sublimative state and structure of Arrokoth at the dawn of the Quiescent Period, regardless of whether such unobservable layers exist.



### III. Sublimative Spin-State Evolution

Sublimative outgassing of volatiles can produce torques that change an object's rotation state. Since Arrokoth is thought to have formed from the accretion of two lobes to form the bilobate shape observed by the *New Horizons* spacecraft, sublimative torques may have played a role in spinning down the lobes to facilitate merger (*McKinnon et al. 2020*) or spinning up the object to separate the lobes (*Hirabayashi et al. 2020*). However, the effects of sublimation early in

Arrokoth’s history (e.g., immediately after the clearing of the PPD) are much stronger than later in Arrokoth’s history, due to supervolatiles being readily available near its surface. This requires that we explore these two regimes separately. Here we explore the limits and effects of such sublimative torques on the rotation state of Arrokoth.

To compute how such outgassing may change the rotation rate of Arrokoth, we use the SYORP sublimative torque model (*Steckloff & Jacobson, 2016; Steckloff & Samarasinha, 2018*), which repurposes the mathematical machinery of the YORP effect (taking advantage of the similarities in the behavior of radiative and sublimative processes). From this model, the maximum sublimative angular acceleration of Arrokoth is

$$\left| \frac{d\omega}{dt} \right| = \frac{3P_S C_S}{4\pi\rho R^2} \quad (6)$$

$$= \frac{3\Phi_{sub} m v_{thermal} C_S}{4\pi\rho R^2} \quad (7)$$

where  $P_S$  is the dynamic sublimation pressure exerted by the escaping gases on the surface,  $C_S$  is an empirical factor analogous to YORP coefficients,  $\rho$  is the bulk density of Arrokoth;  $R$  is the mean radius of Arrokoth, approximately 8.5 km (*Stern et al. 2019*),  $\Phi_{sub}$  is the sublimative gas flux from the surface,  $m$  is the molecular mass of the volatile, and  $v_{thermal}$  is the mean molecular thermal velocity of the molecule. This model assumes that the object has a very low albedo (consistent with the 6.3% bond albedo of Arrokoth [*Hofgartner et al. 2020*]), and is composed entirely of a single volatile ice (for example, CO). This model also assumes that the multiple different chemical species composing Arrokoth do not interact with one another. Such interactions can change molecular binding energies, and thus latent heats of sublimation. However, such effects are poorly understood, and beyond the current state of the art of comet science. Note that this equation only provides the magnitude of the angular acceleration, and that sublimative torques could spin the object up or down.

Like the YORP coefficients (*Scheeres, 2007; Rozitis & Green, 2013*), the SYORP coefficient  $C_S$  parameterizes how a body’s spin pole obliquity and irregular shape leads to net torques (*Steckloff & Jacobson, 2016*). Unlike radiative processes in which the entire surface emits photons, much of the surfaces of icy bodies are sublimatively inactive. Thus, the SYORP coefficient  $C_S$  also accounts for the effects of volatile distribution on sublimative torques (*Steckloff & Samarasinha, 2018*). Additionally, SYORP coefficients must account for the collisional nature of gas molecules near the surfaces of icy bodies, which will cause gas molecules to spread out and

collide with the surface, weakening the sublimative generation of torques. Pristine icy objects may have SYORP coefficients on the order of  $\sim 0.0001 - 0.001$  (Steckloff & Jacobson, 2016), which is an order of magnitude lower than the typical range for YORP coefficients (Scheeres, 2007; Rozitis & Green, 2013). However, evolved objects with only partially sublimatively active surfaces likely have SYORP coefficients that are lower than this range.

To more accurately model sublimative torques, we use observed rotation state changes in short-period comets to compute the SYORP coefficients for these “real”, evolved objects. We rearrange equation 6 to solve for  $C_S$  from observed rotation state changes and nucleus material properties. In cases where the bulk density of the nucleus is not known, we assume a typical range of comet bulk densities of  $300 - 700 \text{ kg/m}^3$  (Steckloff & Samarasinha, 2018). We compute the SYORP coefficients for comets 2P/Encke, 9P/Tempel 1, 10P/Tempel 2, 19P/Borrelly, 67P/Churyumov-Gerasimenko, and 103P/Hartley 2, and find that they span a relatively narrow range of values,  $1.22 \times 10^{-5} - 8.43 \times 10^{-5}$  (see Table 1).

We use these values to compute the effects of CO sublimative torques on Arrokoth shortly after formation (see figure 2), with the timescale of Arrokoth’s changing rotation period depending

	Dominant Volatile species	Effective Radius (km)	Bulk Density ( $\text{kg/m}^3$ )	Rotation period (hr)	Observed Change in Rotation Period (min)	Computed SYORP Coefficient ( $C_S$ )
2P/Encke	H <sub>2</sub> O	2.4 <sup>[a][b]</sup>	300-700(assumed) <sup>[c]</sup>	11 <sup>[a][b]</sup>	4 <sup>[a][b]</sup>	$(3.7 - 8.6) \times 10^{-5}$
9P/Tempel 1	H <sub>2</sub> O	2.83 <sup>[a][b]</sup>	470 <sup>+780</sup> <sub>-230</sub> <sup>[d][e]</sup>	41 <sup>[a][b]</sup>	14 <sup>[a][b]</sup>	$1.22^{+2.03}_{-0.60} \times 10^{-5}$
10P/Tempel 2	H <sub>2</sub> O	6.0 <sup>[a][b]</sup>	300-700(assumed) <sup>[c]</sup>	9 <sup>[a][b]</sup>	0.27 <sup>[a][b]</sup>	$(1.4 - 3.3) \times 10^{-5}$
19P/Borrelly	H <sub>2</sub> O	2.52 <sup>[b]</sup>	560 $\pm$ 270 <sup>[f]</sup>	28 <sup>[b]</sup>	40 <sup>[b]</sup>	$7.27(\pm 3.50) \times 10^{-5}$
67P/Churyumov-Gerasimenko	H <sub>2</sub> O	1.65 <sup>[b]</sup>	533 $\pm$ 6 <sup>[g]</sup>	12 <sup>[b]</sup>	21 <sup>[b]</sup>	$8.43(\pm 0.09) \times 10^{-5}$
103P/Hartley 2	CO <sub>2</sub>	0.58 <sup>[a][b]</sup>	300 $\pm$ 100 <sup>[h]</sup>	18 <sup>[a][b]</sup>	150 <sup>[a][b]</sup>	$1.70(\pm 0.57) \times 10^{-5}$

**Table 1:** Observed parameters of Jupiter-Family comets, used to compute SYORP coefficients. The SYORP coefficient  $C_S$  is a parameter that can be computed from observations and properties of comet nuclei. We find that the SYORP coefficients are 1-2 orders of magnitude smaller than those for pristine icy objects (Steckloff & Jacobson, 2016), and 2-3 orders of magnitude smaller than the analogous YORP coefficients for radiative torques (Scheeres, 2007; Rozitis & Green, 2013).

References: [a] Samarasinha & Mueller (2013), [b] Mueller & Samarasinha (2018), [c] reasonable range of cometary bulk densities (Steckloff & Samarasinha, 2018), [d] Richardson et al. (2007), [e] Thomas et al. (2013), [f] Farnham & Cochran (2002), [g] Pätzold et al. (2016), [h] Thomas et al. (2013)

on bulk density and efficiency of the sublimative torques (i.e., the SYORP coefficient  $C_S$ ). We assume a bulk density for Arrokoth of between 300 – 500 kg/m<sup>3</sup> (Hirabayashi et al. 2020; consistent with McKinnon et al. 2020). The higher end of this plausible density range (500 kg/m<sup>3</sup>; Hirabayashi et al. 2020; McKinnon et al. 2020) is typical of Jupiter Family Comets such as 67P/Churyumov-Gerasimenko (Pätzold et al. 2016) or (D/1993 F2) Shoemaker-Levy 9 (Asphaug & Benz, 1996). At this density, Arrokoth’s lobes would separate at a spin period of 12.5 hours (Hirabayashi et al. 2020), and sublimative torques would require ~0.1 – 10 Myr to spin down Arrokoth to its present 15.92 hour spin period (assuming its maximum outgassing rate). However, such an outgassing rate would deplete Arrokoth of CO in only ~10,000 years. As a result,

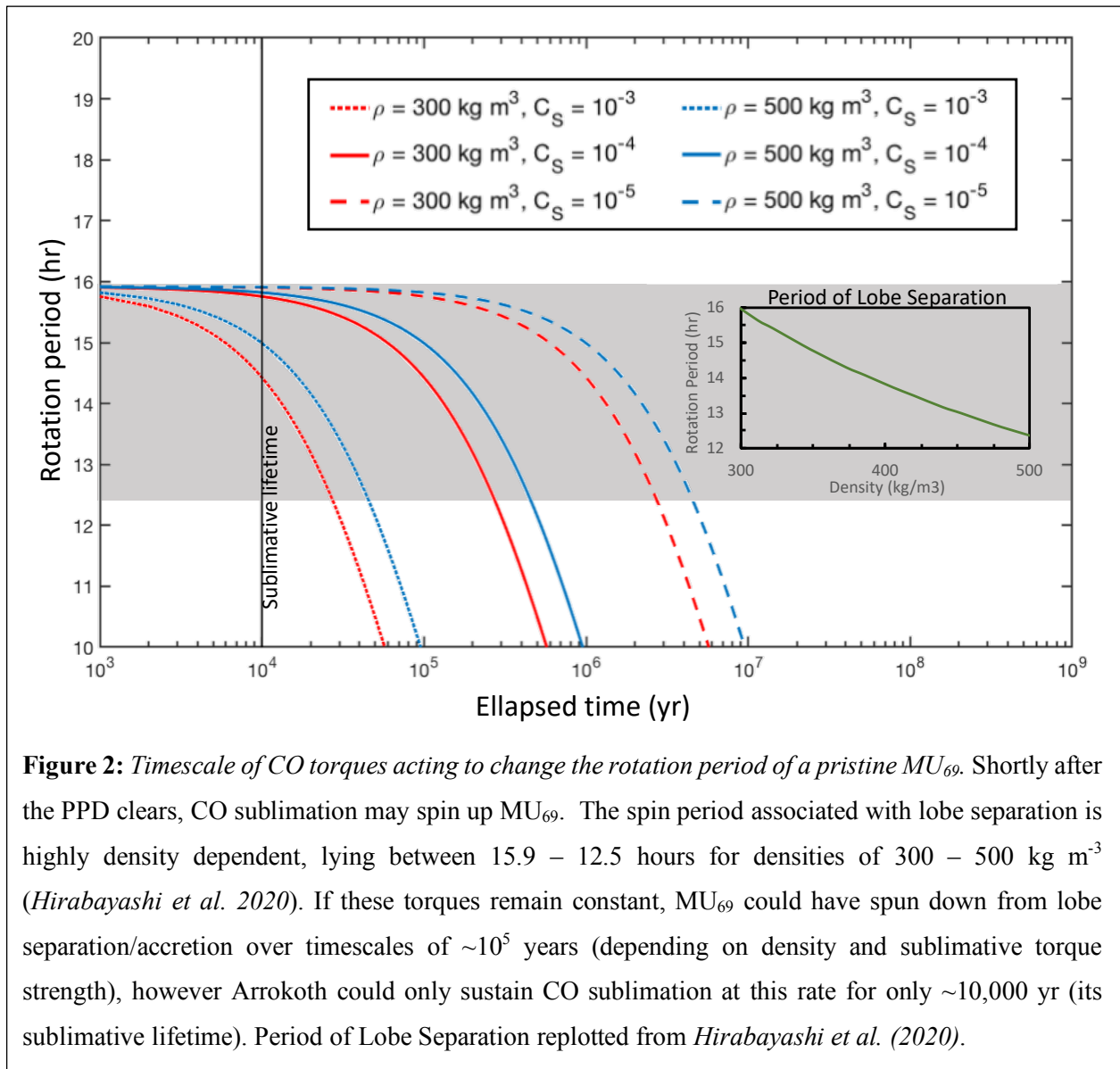


**Figure 2:** Timescale of CO torques acting to change the rotation period of a pristine MU<sub>69</sub>. Shortly after the PPD clears, CO sublimation may spin up MU<sub>69</sub>. The spin period associated with lobe separation is highly density dependent, lying between 15.9 – 12.5 hours for densities of 300 – 500 kg m<sup>-3</sup> (Hirabayashi et al. 2020). If these torques remain constant, MU<sub>69</sub> could have spun down from lobe separation/accretion over timescales of ~10<sup>5</sup> years (depending on density and sublimative torque strength), however Arrokoth could only sustain CO sublimation at this rate for only ~10,000 yr (its sublimative lifetime). Period of Lobe Separation replotted from Hirabayashi et al. (2020).

sublimative torques would have changed Arrokoth’s rotation period by only as many as a few minutes to tens of minutes (depending on density and SYORP coefficient).

Although these timescales imagine a maximally outgassing Arrokoth, in reality such volatile loss rates would slow down as the sublimation front receded below the surface, allowing outgassing to last until the solar thermal wave reaches Arrokoth’s center (the entire length of the sublimative period). Nevertheless, our modeling effort depends solely on the total volatile flux; the outgassing rate and duration are irrelevant over secular timescales so long as the total volatile flux is the same.

Arrokoth’s shape is minimally stable at the lower end of its range of plausible densities of  $\sim 300 - 500 \text{ kg/m}^3$  (Hirabayashi *et al.* 2020; McKinnon *et al.* 2020), a density consistent with the density of comet 103P/Hartley 2 (Thomas *et al.* 2013; Richardson & Bowling, 2014). At such densities, Arrokoth’s lobes separate at spin periods just below its present-day spin period; and sublimative torques could have caused the lobes to separate. However, at densities of even a few  $\sim 10$ ’s of  $\text{kg/m}^3$  above this lower limit, sublimative torques would be insufficient to change Arrokoth’s spin state sufficiently to cause its lobes to separate. Ultimately, sublimative torques are unlikely to have a significant effect on Arrokoth’s spin state during the Sublimative Period, changing its spin period by a few minutes at most, before vigorous sublimation ceases.

Outgassing during Arrokoth’s Quiescent Period similarly had a negligible effect on Arrokoth’s spin state. We rearrange equation 7 to solve for the flux required to spin the nucleus up/down

$$\Phi_{sub} = \frac{4\pi\rho R^2\Delta\omega}{3mv_{thermal}c_s\Delta t} \quad (8)$$

where  $\Delta t$  is the duration of volatile sublimation (here 4.5 billion years) and  $\Delta\omega$  is the change in angular speed, which we set to  $10^{-6}$  to represent spin period changes on the order of a few minutes (comparable to the limit in the Sublimative Period). We use best-case parameters for Arrokoth to compute the lowest sublimative flux needed for this change: low density of  $300 \text{ kg/m}^3$  (Hirabayashi *et al.* 2020; McKinnon *et al.* 2020), peak temperature of  $58 \text{ K}$  (Grundy *et al.* 2020) across the body, and high SYORP coefficient of  $10^{-4}$ . Even with these best-case values, the average  $\text{CO}_2$  flux from Arrokoth would need to be  $\sim 10^{17}$  molecules/s to change its spin period by a few minutes. However, the sublimative flux of  $\text{CO}_2$ , the most volatile major component of cometary ices following  $\text{CO}$ , would have a maximum flux from Arrokoth of only  $\sim 10^{11}$  molecules/s (figure 1). For lower SYORP values and higher bulk densities (which are more

consistent with other typical Cold Classical Kuiper Belt Object density estimates of  $\sim 600 - 1400$   $\text{kg/m}^3$ ; *Vilenius et al. 2012*; *Grundy et al. 2012*; *Brown, 2013*; *Vilenius et al. 2014*), the minimum flux increases to  $\sim 10^{18}$  molecules/s. Other, more volatile ices may contribute to this flux, but would have minor contributions. Thus, Arrokoth's spin state has changed negligibly since the end of the Sublimative Period.

Finally, we have thus far treated sublimative torques as monotonic increases or decreases in the rotation state of an object. However, sublimative torques are likely stochastic in direction, both spinning objects up and down (*Statler, 2009*; *Cotto-Figueroa et al. 2015*). With this consideration, the calculated changes in rotation rates may overestimate actual changes by an order of magnitude.

Considering that impacts have also changed Arrokoth's spin period by at most a few minutes (*Hirabayashi et al. 2020*), the present spin period is representative of Arrokoth's spin state upon the clearing of the Sun's protoplanetary disk. Similarly, sublimative torques are unlikely to have contributed to the initial formation of Arrokoth's contact binary shape. Arrokoth's shape is indicative of a gentle merger of the two lobes, suggesting a gentle process for eliminating orbital angular momentum from the system to cause the lobes to merge (*McKinnon et al. 2020*), such as nebular drag (*McKinnon et al. 2020*; *Lyra et al. 2020 submitted*). Sublimative torques can only change the present angular momentum of the Arrokoth system by less than  $\sim 1\%$  (assuming ideal conditions), and therefore contributed negligibly to the initial merger of Arrokoth's lobes. This further supports the notion that Arrokoth's shape is primordial (*McKinnon et al. 2020*).

#### IV. Sublimative Surface Evolution

Volatile sublimation can drive topographic erosion (*Britt et al. 2004*; *Steckloff & Samarasinha, 2018*) and mass transport about the surface of an icy body (*Lai et al. 2016*). Rates of sublimation-driven erosion/deposition likely vary significantly within classes of icy bodies, and between different dynamical classes of bodies. Although a full calculation of these erosion/deposition rates on Arrokoth would require detailed simulations with many underconstrained variables. Nevertheless, if we assume that sublimation-driven evolution of Jupiter Family Comets is representative (when scaled) of icy bodies in the solar system, we can use existing studies of mass transport on JFCs to estimate the magnitude of mass transport/deposition on Arrokoth.

During the sublimative era, the surface vigorously sublimated CO and other supervolatiles. Using the sublimation model of *Steckloff et al. (2015)*, we find that, even though CO is significantly more volatile than H<sub>2</sub>O ice, the dynamic sublimation pressure driving and transporting dust about Arrokoth's surface is only ~0.5% as strong as H<sub>2</sub>O's dynamic sublimation pressure on a typical JFC. Additionally, Arrokoth's large size gives it a surface escape speed and surface gravity on the order of 5 times greater than those of a typical JFC such as 67P/Churyumov-Gerasimenko (assuming comparable densities). Comparing these weak drag forces and higher gravity, the maximum loftable dust grain from Arrokoth would be ~0.1% the radius of the maximum loftable grain on 67P/Churyumov-Gerasimenko (on the order of hundreds of microns, rather than on the order of decimeters; *Lai et al. 2016; Keller et al. 2017*).

The grain size frequency distribution modeled in *Lai et al. (2016)* has a break in the power law differential size-frequency distribution at around a millimeter, with grains smaller than this following a power-law index of 2, and grains larger than this following a power-law index of 4 (a steeper drop-off with size (a power-law index of 3 indicates that mass is equally distributed amongst the grain sizes). Therefore, less mass is in the population of larger grains than in the population of smaller grains. Thus, if a similar grain-size distribution held true on Arrokoth, then the loss of these larger grains (which cannot be lofted on Arrokoth) would reduce the transported mass per unit area by less than 0.1% (relative to 67P). We adopt a 0.1% value as a conservative estimate.

Numerical models of thermally driven erosion and deposition are highly sensitive to model parameters. Nevertheless, numerous models explored the role of such processes on comet 67P/Churyumov-Gerasimenko, a Jupiter-Family Comet that was the target of the *Rosetta* mission, and found broad agreement in erosion/deposition rates. Global models found that the surface of 67P/Churyumov-Gerasimenko can erode on the order of ~4 m/year (*Lai et al. 2016; Keller et al. 2017*), and experience depositional growth on the order of ~0.5 m/yr (*Lai et al. 2016*) during an apparition. This is consistent with analysis of *Rosetta* images, which suggest erosion in many region of ~1 m and deposition of around ~20 cm (*Xu et al. 2017*). Other modeling efforts find that smooth terrains on 67P/Churyumov-Gerasimenko experience topographic evolution of ~1 m or less (*Tang et al. 2019*) or ~20 cm (*Kossacki & Jasiak, 2019*), although these terrains are themselves depositional, and can experience subsequent thermally driven topographic evolution (*Birch et al.*

2019). These results are consistent with the expectation that topographic changes occur more rapidly on steeper terrains than flatter terrains (*Steckloff et al. 2018*).

Ultimately, these studies suggest that the erosion rate on comet 67P/Churyumov-Gerasimenko is on the order of  $\sim 0.2 - 4$  m/year; thus, the scaled erosion rate on Arrokoth would be  $\sim 0.02 - 0.4$  cm/yr. Arrokoth's higher escape speed and weaker sublimation pressures would result in negligible grain escape (unlike Jupiter family comets), resulting in a deposition rate that effectively matches the erosion rate. Thus, over the sublimative lifetime of Arrokoth (the time in which a block of CO the size of Arrokoth would completely disappear) of  $\sim 10,000$  yr, the topography may erode/fill in, and ultimately change by as much as  $\sim 10 - 100$  m during the sublimative period.

By comparison, sublimative forces during the quiescent period are effectively non-existent. The outgassing constraint observed by the *New Horizons* spacecraft would result in sublimation pressures more than 13 orders of magnitude smaller than those during the Sublimative Period. Dust transport under such conditions would undoubtedly be negligible, consistent with the lack of an observable dust coma during the *New Horizons* flyby.

These mass transport processes could profoundly alter the primordial surface of Arrokoth. Such erosion and deposition could effectively erase craters up to  $\sim 50 - 500$  m across (assuming canonical depth/diameter ratio of 0.2). Indeed, most of the observed and suspected craters on Arrokoth fall in the upper end of this size range (*Spencer et al. 2020*). This suggests, rather provocatively, that the majority of the observed surface morphology and craters on Arrokoth may not date not from the Sublimative Period, but rather from the Quiescent Period. In other words, although Arrokoth's shape is likely primordial, its surface may not be.

## V. Conclusions

We consider the effects of sublimating volatiles on (486958) Arrokoth, and find that Arrokoth's sublimative history can be separated into two periods. An early Sublimative Period lasting  $\sim 10-100$  Myr after the clearing of the Sun's protoplanetary disk (PPD), during which Arrokoth's supervolatile species such as CO sublimated vigorously. Such sublimation would cause significant erosion and dust transport about the surface, erasing surface features shallower than  $\sim 10 - 100$  m. This includes craters up to  $\sim 50 - 500$  m across, suggesting that the surface of Arrokoth we see today may not be primordial, but rather could date from after the Sublimative Period. Arrokoth's Sublimative Period was followed by a Quiescent Period, which continues to the present

day. The Quiescent Period is marked by a lack of significant outgassing, with expected volatile production rates at least 13 orders of magnitude smaller than what *New Horizons* could detect. Sublimative torques have been insignificant throughout Arrokoth's history, suggesting that the present spin rate is representative of Arrokoth's primordial spin state, and that Arrokoth's shape, unlike its surface, is indeed primordial.

## VI. Acknowledgments

The authors wish to thank Seth Jacobson for productive conversations that helped explore the implications of this work. The authors also wish to thank both anonymous reviewers, whose comments greatly improved the content, structure, organization, and ultimately, the conclusions and implications of this work. J.K.S. and G.S. acknowledge support from NASA award 80NSSC18K0497.

## VII. References

- Asphaug, E.; Benz, W. (1996) Size, density, and structure of Comet Shoemaker-Levy 9 Inferred from the physics of tidal breakup. *Icarus* **121**, 225–248
- Birch, S.P.D.; Hayes, A.G.; Umurhan, O.; Tang, M.; Vincent, J.-B. et al. (2019) Migrating scarps as a significant driver for cometary surface evolution. *GRL* **46**(22), 12794 – 12804
- Britt, D.T.; Boice, D.C.; Buratti, B.J.; Campins, H.; Nelson, R.M. et al. (2004) The morphology and surface processes of Comet 19/P Borrelly, *Icarus* **167**, 45 - 53
- Brown, M.E. (2013) The density of mid-sized Kuiper Belt object 2002 UX25 and the formation of the dwarf planets. *ApJ* **778**:L34 (5pp)
- Choi, Y.-J.; Cohen, M.; Merk, R.; Prrialnik, D. (2002) Long-Term Evolution of Objects in the Kuiper Belt Zone – Effects of Insolation and Radiogenic Heating. *Icarus* **160**(2), 300 - 312
- Cotto-Figueroa, D.; Statler, T.S.; Richardson, D.C.; Tanga, P. (2015) Coupled spin and shape evolution of small rubble-pile asteroids: Self-limitation of the YORP effect. *ApJ* **803**:25 (18pp.)
- Davidsson, B.J.R.; Sierks, H.; Güttler, C.; Marzari, F.; Pajola, M., et al. (2016) The primordial nucleus of comet 67P/Churyumov-Gerasimenko. *A&A* **592**, A63 (30pp)

- Desch, S.J.; Cook, J.C.; Doggett, T.C.; Porter, S.B. (2009) Thermal evolution of Kuiper belt objects, with implications for cryovolcanism. *Icarus* **202**, 694 - 714
- Drury, M.J. (1987) Thermal diffusivity of some crystalline rocks. *Geothermics* **16**(2), 105 - 115
- Farnham, T.L., Cochran, A.L. (2002) A McDonald observatory study of comet 19P/Borrelly: placing the deep space 1 observations into a broader context. *Icarus* **160**, 398–418.
- Grundy, W.M.; Benecchi, S.D.; Raninowitz, D.L.; Porter, S.B.; Wasserman, L.H. et al. (2012) Mutual events in the Cold Classical transneptunian binary system Sila and Nunam. *Icarus* **220**, 74 – 83
- Grundy, W.M.; Bird, M.K.; Britt, D.T.; Cook, J.C.; Cruikshank, D.P.; et al. (2020) Color, composition, and thermal environment of Kuiper Belt object (486958) Arrokoth. *Science* aay3705 (12 pp.) doi: 10.1126/science.aay3705
- Guilbert-Lepoutre, A.; Lasue, J.; Federico, C.; Coradini, A.; Orosei, R.; Rosenberg, E.D. (2011) New 3D thermal evolution model for icy bodies application to trans-Neptunian objects. *A&A* **529**, A71 (11 pp.) doi: [10.1051/0004-6361/201014194](https://doi.org/10.1051/0004-6361/201014194)
- Guilbert-Lepoutre, A.; Rosenberg, E.D.; Prialnik, D.; Besse, S. (2016) Modelling the evolution of a comet subsurface: implications for 67P/Churyumov-Gerasimenko. *MNRAS* **462**, S146 – S155 doi: [10.1093/mnras/stw2371](https://doi.org/10.1093/mnras/stw2371)
- Gundlach, B.; Blum, J. (2012) Outgassing of icy bodies in the Solar System – II: Heat transport in dry, porous surface dust layers. *Icarus* **219**, 618 - 629
- Hirabayashi, M.; Scheeres, D.J.; Chesley, S.R.; Marchi, S.; McMahon, J.W. et al. (2016) Fission and reconfiguration of bilobate comets as revealed by 67P/Churyumov-Gerasimenko. *Nature* **534**, 352 – 355
- Hirabayashi, M.; Trowbridge, A.J.; Bodewits, D. (2020). The Mysterious Location of Maryland on 2014 MU69 and the Reconfiguration of Its Bilobate Shape. *ApJL* **89**:L12 (6pp)
- Hofgartner, J.D.; Burati, B.J.; Benecchi, S.D.; Beyer, R.A.; Cheng, A. et al. (2020) Photometry of Kuiper belt object (486958) Arrokoth from New Horizons LORRI. *Icarus* In press. 2 March, 2020
- Hu, X.; Shi, X.; Sierks, H.; Fulle, M.; Blum, J. et al. (2017) Seasonal erosion and restoration of the dust cover on comet 67P/Churyumov-Gerasimenko as observed by OSIRIS onboard Rosetta. *A&A* **604**, A114 (31 pp.)

- Keller, H.U.; Mottola, S.; Hviid, S.F.; Agarwal, J.; Kührt, E. et al. (2017) Seasonal mass transfer on the nucleus of comet 67P/Churyumov-Gerasimenko. *MNRAS* **469**, S357 – S371
- Kokotanekova, R.; Snodgrass, C.; Lacerda, P.; Green, S.F.; Lowry, S.C.; Fernández, Y.R. et al. (2017) Rotation of cometary nuclei: new light curves and an update of the ensemble properties of Jupiter-family comets. *MNRAS* **471**(3), 2974 - 3007
- Kossacki, K.J.; Jasiak, A. (2019) The evolution of gently sloping mantled deposits on Comet 67P/Churyumov-Gerasimenko. *Icarus* **319**, 381 – 391 doi: [10.1016/j.icarus.2018.09.035](https://doi.org/10.1016/j.icarus.2018.09.035)
- Krijt, S.; Schwarz, K.R.; Bergin, E.A.; Ciesla, F.J. (2018) Transport of CO in protoplanetary disks: consequences of pebble formation, settling, and radial drift. *ApJ* **864**, 78 (18 pp.) The Astrophysical Journal, 864:78 (18pp), doi: 10.3847/1538-4357/aad69b
- Lai, I.L.; Ip, W.H.; Su, C.C.; Wu, J.S.; Lee, J.C. et al. (2016) Gas outflow and dust transport of comet 67P/Churyumov-Gerasimenko. *MNRAS* **462**, S533 – S546
- Langmuir, I. (1913) The vapor pressure of metallic tungsten. *Phys. Rev. II* (5), 329 - 342
- Lisse, C.M.; Young, L.A.; Cruikshank, D.P.; Sandford, S.A.; Stern, S.A. et al. (2020) On the stability of KBO 2014 MU<sub>69</sub>'s Ices. *Icarus*. This issue
- Lyra, W.; Youdin, A.N.; Johansen, A.; Umurhan, O.M. (2020) Evolution of MU69 from a binary planetesimal into contact by Kozai-Lidov Oscillations and Nebular Drag. *Icarus*. In revision
- Marshall, D.; Groussin, O.; Vincent, J.-B.; Brouet, Y.; Kappel, D. et al. (2018) Thermal inertia and roughness of the nucleus of comet 67P/Churyumov-Gerasimenko from MIRO and VIRTIS observations. *A&A* **616**, A122 (13 pp.) DOI: [10.1051/0004-6361/201833104](https://doi.org/10.1051/0004-6361/201833104)
- McKinnon, W.B.; Richardson, D.C.; Marohnic, J.C.; Keane, J.T.; Grundy, W.M. et al. (2020) The solar nebula origin of (486958) Arrokoth, a primordial contact binary in the Kuiper Belt. *Science* 10.1126/science/aay6620
- Merk, R.; Prialnik, D. (2003) Early Thermal and Structural Evolution of Small Bodies in the Trans-Neptunian Zone. *Earth, Moon, and Planets* **92**, 359 - 374
- Mueller, B.E.A., Samarasinha, N.H. (2018) Further investigation of changes in cometary rotation. *AJ* **156**:107 (7pp.)
- Pätzold, M., Andert, T., Hahn, M., Asmar, S.W., Barriot, J.P., et al. (2016) A homogeneous nucleus for comet 67P/Churyumov-Gerasimenko from its gravity field. *Nature* **530**, 63–65.

- Preusker, F.; Scholten, F.; Matz, K.-D.; Roatsch, T.; Hviid, S.F. *et al.* (2017) The global meter-level shape model of comet 67P/Churyumov-Gerasimenko. *A&A* **607**, L1 (5 pp.) DOI: [10.1051/0004-6361/201731798](https://doi.org/10.1051/0004-6361/201731798)
- Prialnik, D.; Benkhoff, J.; Podolak, M. (2004) Modeling the structure and activity of comet nuclei. In *Comets II*, 359 – 387
- Prialnik, D.; Podolak, M. (1995) Radioactive Heating of Porous Comet Nuclei. *Icarus* **117**, 420 - 430
- Prialnik, D.; Sarid, G.; Rosenberg, E.D.; Merk, R. (2008) Thermal and Chemical Evolution of Comet Nuclei and Kuiper Belt Objects. *Space Science Reviews* **138**, 147 - 164
- Richardson, J.E.; Melosh, H.J.; Lisse, C.M.; Carcich, B. (2007) A ballistics analysis of the Deep Impact ejecta plume: Determining Comet Tempel 1's gravity, mass, and density. *Icarus* **190**, 357 - 390
- Richardson, J.E., Bowling, T.J. (2014) Investigating the combined effect of shape, density, and rotation on small body surface slopes and erosion rates. *Icarus* **234**, 53–65
- Rosenberg, E.D.; Prialnik, D. (2010) The effect of internal inhomogeneity on the activity of comet nuclei – Application to Comet 67P/Churyumov-Gerasimenko. *Icarus* **209**(2), 753 - 765
- Rozitis, B., Green, S.F., 2013. The influence of global self-heating on the Yarkovsky and YORP Effects. *Mon. Not. R. Astron. Soc.* **433** (1), 603–621.
- Sagan, C.; Mullen, G. (1972) Earth and Mars: Evolution of Atmospheres and Surface Temperatures. *Science* **177**, 52 - 56
- Samarasinha, N.H., Mueller, B.E.A. (2013) Relating changes in cometary rotation to activity: current status and applications to Comet C/2012 S1 (ISON). *ApJ Letters* **775**, L10 6pp.
- De Sanctis, M.C.; Capria, M.T.; Coradini, A. (2001) Thermal evolution and differentiation of Edgeworth-Kuiper Belt Objects. *AJ* **121**, 2792 – 2799
- De Sanctis, M.C.; Capria, M.T.; Coradini, A.; Ammannito, E. (2007) Thermal evolution models of the 9P/Tempel 1 comet nucleus for interpreting the Deep Impact results. *AJ* **133**, 1836 - 1846
- Sarid, G.; Prialnik, D. (2009) From KBOs to Centaurs: The thermal connection. *Meteoritics & Planetary Science* **44**, 1905 - 1916

- Scheeres, D.J. (2007) The dynamical evolution of uniformly rotating asteroids subject to YORP. *Icarus* **188**, 430–450.
- Spencer, J.R.; Stern, S.A.; Moore, J.M.; Weaver, H.A.; Singer, K.N. *et al.* (2020) The geology and geophysics of Kuiper Belt object (486958) Arrokoth. *Science* aay3999 (12 pp.) doi:10.1126/science.aay3999
- Statler, T.S. (2009) Extreme sensitivity of the YORP effect to small-scale topography. *Icarus* **202**, 502 - 513
- Steckloff, J.K.; Johnson, B.C.; Bowling, T.; Melosh, H.J.; Minton, D.; Lisse, C.M.; Battams, K. (2015) Dynamic sublimation pressure and the catastrophic breakup of Comet ISON. *Icarus* **258**, 430 - 437
- Steckloff, J.K.; Jacobson, S.A. (2016) The formation of striae within cometary dust tails by a sublimation-driven YORP-like effect. *Icarus* **264**, 160 - 171
- Steckloff, J.K.; Samarasinha, N.H. (2018) The sublimative torques of Jupiter Family Comets and mass wasting events on their nuclei. *Icarus* **312**, 172 – 180
- Stern, S.A.; Weaver, H.A.; Spencer, J.R.; Olkin, C.B.; Gladstone, G.R.; Grundy, W.M. *et al.* (2019) Initial results from the New Horizons exploration of 2014 MU<sub>69</sub>, a small Kuiper Belt objects. *Science* **364**, eaaw9771 (12 pp.)
- Tang, Y.; Birch, S.P.D.; Hayes, A.G.; Kirk, R.; Kutsop, N. (2019) Generation of photoclinometric DTMs for application to transient changes on the surface of comet 67P/Churyumov-Gerasimenko. *A&A* **630**, A10 (8 pp.) DOI: [10.1051/0004-6361/201834127](https://doi.org/10.1051/0004-6361/201834127)
- Thomas, P. *et al.* (2013) The nucleus of Comet 9P/Tempel 1: Shape and geology from two flybys. *Icarus* **222**, 453 - 466
- Thomas, P.C., *et al.* (2013) Shape, density, and geology of the nucleus of comet 103P/Hartley 2. *Icarus* **222**, 550–558.
- Vilenius, W.; Kiss, C.; Mommert, M.; Müller, T.; Santos-Sanz, P. *et al.* (2012) “TNOs are Cool”: A survey of the trans-Neptunian region VI. Herschel/PACS observations and thermal modeling of 19 classical Kuiper belt objects. *A&A* **541**, A94 (17 pp)
- Vilenius, E.; Kiss, C.; Müller, T.; Mommert, M.; Santos-Sanz, P. *et al.* (2014) “TNOs are Cool”: A survey of the trans-Neptunian region. X. Analysis of classical Kuiper belt objects from Herschel and Spitzer observations. *A&A* **564**, A35 (18 pp.)

Williams, J.P.; Cieza, L.A. (2011) Protoplanetary Disks and Their Evolution. *Annual Review of Astronomy and Astrophysics* **49**, 67 - 117